Self-consistency and universality of camera lens distortion models

April 5, 2011

Abstract

This paper introduces the concepts of "self-consistency" and "universality" to evaluate the validity and precision of camera lens distortion models. Self-consistency is evaluated by the residual error when the distortion generated with a certain model is corrected by the best parameters for the same model (used in reverse way). Analogously, universality is measured by the residual error when a model is used to correct distortions generated by a family of other models. Five classic camera lens distortion models are reviewed and compared for their degree of self-consistency and universality. The study shows that radial symmetric models can be self-consistent, but cannot be used for non radial-symmetric distortion. Among the evaluated models, the polynomial and the rational models are the only ones to be universal up to precisions of 1/100 pixel. However, the polynomial model, being linear, is much simpler and faster to estimate. Unusually high polynomial orders are required to reach a 1/100 pixel precision. But our experiments show that such polynomials are easily computed, producing a precise lens distortion correction without over-fitting. Our conclusions are validated by three independent experimental setups: The models are compared first in synthetic experiments by their approximation power; second by fitting a real camera distortion estimated by a non parametric algorithm; and finally by the absolute correction measurement provided by photographs of tightly stretched strings, warranting a high straightness.

1 Introduction

The pinhole camera model is widely used in computer vision applications because of its simplicity and its linearity in terms of projective geometry [13]. But real cameras deviate from the ideal pinhole model, mainly because of lens distortion [2]. Thus an accurate camera lens distortion correction is the first step towards high precision 3D metric reconstruction from photographs. With the steady progress in lens quality and computing power, high-precision 3D reconstructions become feasible, demanding in turn higher lens distortion precisions

than those provided by classic methods. The object of this paper is to investigate the validity of distortion models at the light of precision requirements increased by two to three orders of magnitude. This increased accuracy requires a new methodology for evaluating distortion models. In a nutshell, our conclusion is that a polynomial model of higher degree than usual, ranging from 8 to 15, is necessary for reaching a pixel precision ranging from 1/100 to 1/1000. The polynomial model permits to approximate at this resolution any other model, and the inverse of any other model, including itself. When these properties are reached, the model is called *universal* and *self-consistent*. Among the other four models which will be compared (radial, division, FOV, and rational), only the rational model has the exigible self-consistency and universality, but to a far higher computational cost (a complexe incremental minimization algortihm is needed to solve the rational model, without ensuring the global minima).

Since the first lens distortion model by Brown [2], many methods [16, 29] have been proposed to correct lens distortion (see [24] for a review of the development of camera calibration methods in early years). The final aim is to obtain an ideal pinhole (or pinhole equivalent) camera by removing lens distortion, so that the classic multi-view geometry techniques can be applied directly.

With the exception of a few non-parametric methods [9, 6, 11], an appropriate distortion model is indispensable to establish a correct camera model. The main distortion models are the radial model [2], the division model [10], the FOV model [8], the bicubic model [14], the rational model [5, 12]. This diversity is only marginally linked to the kind of camera. Thus, a synthetic quantitative and qualitative comparison is required. Do these models reflect camera lens distortion in its physical aspect? It could be argued that a correct model should originate from physical measurements on systems of lenses. Surprisingly enough, there is little physical background for the distortion models in the literature. It is true that in [28] lens distortion is decomposed into three effects: radial distortion, decentering distortion and thin prism distortion. But, still, it is only marginally based on a physical background. In fact, the final distortion includes effects caused by a complex lens system, by the camera geometry, and by the (not perfectly planar) shape of the captor. One is therefore led to figure out a flexible model with enough parameters to approximate any plausible distortion. In absence of a physical model, the model classification approach adopted here will be to look for models which actually cope with any other proposed distortion model, at a given precision. The second question is the relationship between the distortion and the correction model, which should be inverse of each other. Indeed, the *correction model* and the *distortion model* must be different. A correction model is used to correct distorted images, while a distortion model is used to model the distortion of ideal images. In the literature, however, it seems that the roles of *distorted point* and *undistorted point* are interchangeable, which again confirms the lack of physical meaning for these models. For example, direct distortion

models are used in global camera calibration [27, 31, 17, 28]. Yet, in most plumb-line methods [2, 8, 1, 21, 26, 4] or some pattern-free methods [23, 30, 10, 18, 25, 5, 20, 3, 15], the very same correction models are used without any fuss to approximate the inverse distortion.

Assume we simulate a camera lens distortion with a certain model and a certain set of parameters. Except for some trivial cases, the distortion will not be corrected by using the same model with other parameters, because the model itself is usually not *invertible*. We propose to measure the error incurring when inverting a distortion with the same model as for the distortion. This error when the best correcting parameters are applied will be a measurement of the model *self-consistency*. In other words, self-consistency relates to how well a model is able to correct distortion generated by a model of its own family. Of course the best models should be universal, therefore able to correct distortions generated by other models. We therefore propose to measure a model *universality* as the residual error when this model is used to correct distortion generated by a whole set of different models. A *universal model* is a model for which this error is very small no matter what other (reasonable) distortion model has been applied. A universal model must of course be also self-consistent. Our goal is to identify the least complex universal and self-consistent models.

The various distortion models will be carefully compared on realistic synthetic distortion data permitting to quantify the ideal attainable precision. Then, the same models will be compared on their capacity to fit a real camera lens distortion (estimated by a non-parametric algorithm [11]). Finally, the lens distortion correction accuracy by each model will be evaluated by using the plumb-line approach, with photographs of tightly stretched string, warranting a high straightness, and giving an absolute measure of the correction quality. In short, there will be four different numerical validations of our conclusions.

This paper is organized as follows. Section 2 reviews five classic distortion models. Their self-consistency and universality are evaluated in Section 3 by synthetic experiments. Section 4 and 5 describe the experiments done with real camera lenses. Section 6 is a conclusion.

2 Distortion and Correction models

We start by reviewing the most current models, namely the radial model [2], the division model [10], the FOV model [8], the polynomial model [14], and the rational function model [5, 12]. All of these models are expressed as distortion models, but are actually also used as correction models.

Denote by (x_u, y_u) an undistorted point, (x_d, y_d) the distorted point, (x_c, y_c) the distortion center, $(\bar{x}_u, \bar{y}_u)$ the radial undistorted point and $(\bar{x}_d, \bar{y}_d)$ the radial distorted point where $\bar{x}_u = x_u - x_c$, $\bar{y}_u = y_u - y_c$, $\bar{x}_d = x_d - x_c$ and $\bar{y}_d = y_d - y_c$. The distorted radius is $r_d = \sqrt{\bar{x}_d^2 + \bar{y}_d^2}$ and the undistorted radius $r_u = \sqrt{\bar{x}_u^2 + \bar{y}_u^2}$.

The radial model displaces a point along its radial direction originating at the distortion center. The distorted new radius r_d is a

function of the original radius r_u,

$$r_d = r_u f(r_u) = r_u(k_0 + k_1 r_u + k_2 r_u^2 + \cdots). \tag{1}$$

The parameter k_0 representing a scaling does not introduce distortion. The scaled image is distorted by $k_1, k_2, \cdots$. If $k_1, k_2, \cdots$ are all positive, we have a *pincushion distortion*; if $k_1, k_2, \cdots$ are all negative, a *barrel distortion*. *Mustache distortion* occurs if the signs of $k_1, k_2, \cdots$ are not the same (see Fig. 1).

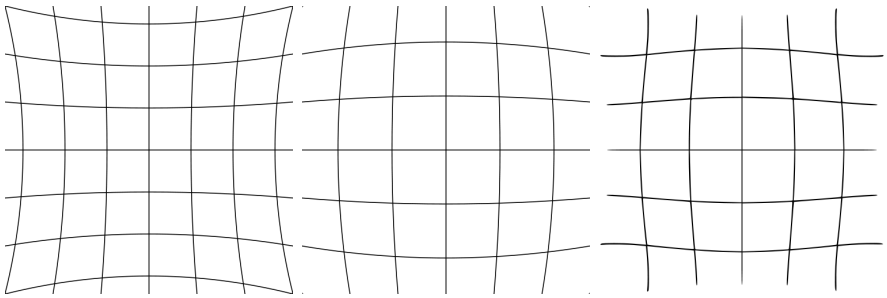

Figure 1: Left: pincushion distortion. Middle: barrel distortion. Right: mustache distortion.

The *division model* is nothing but the scalar inverse of the radial model,

$$r_d = r_u f(r_u) = \frac{r_u}{k_0 + k_1 r_u + k_2 r_u^2 + \cdots}. \tag{2}$$

In these models, the higher order coefficients are needed to model extreme distortion in fish-eye lenses or other wide angle lens systems. A more sparse representation is obtained by parameterizing the distortion by the field of view (FOV). The only parameter of the FOV model is the field of view ω:

$$r_d = r_u f(r_u) = r_u \frac{\tan(r_u \omega)}{2 r_u \tan(\frac{\omega}{2})}. \tag{3}$$

ω is the coeffcient of order 1. More coefficients, like $k_0, k_2, k_3, \cdots$ can be added to FOV model to make it more complete.

In the *polynomial model* the distortion is modeled as a polynomial in $\bar{x}_u$ and $\bar{y}_u$. For example, the third order (bicubic) polynomial model is

$$\begin{aligned} \bar{x}_d &= a_1 \bar{x}_u^3 + a_2 \bar{x}_u^2 \bar{y}_u + a_3 \bar{x}_u \bar{y}_u^2 + a_4 \bar{y}_u^3 + a_5 \bar{x}_u^2 \\ &\quad + a_6 \bar{x}_u \bar{y}_u + a_7 \bar{y}_u^2 + a_8 \bar{x}_u + a_9 \bar{y}_u + a_{10} \\ \bar{y}_d &= b_1 \bar{x}_u^3 + b_2 \bar{x}_u^2 \bar{y}_u + b_3 \bar{x}_u \bar{y}_u^2 + b_4 \bar{y}_u^3 + b_5 \bar{x}_u^2 \\ &\quad + b_6 \bar{x}_u \bar{y}_u + b_7 \bar{y}_u^2 + b_8 \bar{x}_u + b_9 \bar{y}_u + b_{10} \end{aligned} \tag{4}$$

The rational function model is a quotient of two polynomials. A second

order rational function model can be written as

$$\begin{aligned} \bar{x}_d &= \frac{a_1\bar{x}_u^2 + a_2\bar{x}_u\bar{y}_u + \cdots + a_5\bar{y}_u + a_6}{c_1\bar{x}_u^2 + c_2\bar{x}_u\bar{y}_u + \cdots + c_5\bar{y}_u + c_6} \\ \bar{y}_d &= \frac{b_1\bar{x}_u^2 + b_2\bar{x}_u\bar{y}_u + \cdots + b_5\bar{y}_u + b_6}{c_1\bar{x}_u^2 + c_2\bar{x}_u\bar{y}_u + \cdots + c_5\bar{y}_u + c_6} \end{aligned} \tag{5}$$

All of the above models, including the radial model, the division model and the FOV model which are radial symmetric, have the following decomposition in the x and y direction:

$$\begin{aligned} \bar{x}_d &= f_x(\bar{x}_u, \bar{y}_u) \\ \bar{y}_d &= f_y(\bar{x}_u, \bar{y}_u). \end{aligned} \tag{6}$$

The form of f_x and f_y depends on the specific model.

3 Self-consistency and Universality

In the literature it is not always clear whether the above models are correction models or distortion models. If a model can correct itself, we call it *self-consistent*, and *universal* if it can correct others. Both qualities are theoretical properties of the model families. Thus, they can be genuinely evaluated by synthetic experiments. Self-consistency and universality will be tested by generating a distortion with any of the above models, and then evaluating the error incurred when correcting the generated distortion with any of the above models.

3.1 Experiments with known distortion center

We shall first assume that the distortion center (x_c, y_c) is known. To test the self-consistency of a certain model, its direct model in Eq. (6) was used to generate a distortion with realistic coefficients (see Table 1). This distortion was corrected by identifying the best parameters in the same model,

$$\begin{aligned} \bar{x}_u &= g_x(\bar{x}_d, \bar{y}_d) \\ \bar{y}_u &= g_y(\bar{x}_d, \bar{y}_d) \end{aligned} \tag{7}$$

where the form of g_x, g_y depends on the model selected. In the synthetic test, $(\bar{x}_u, \bar{y}_u)$ and $(\bar{x}_d, \bar{y}_d)$ are both known. The unknowns are the parameters of g_x and g_y. So the question is how well we can approach the ideal correction $(\bar{x}_u, \bar{y}_u)$ by $g_x(\bar{x}_d, \bar{y}_d)$ and $g_y(\bar{x}_d, \bar{y}_d)$. We want to compute the coefficients of g_x and g_y by minimizing the difference between the ideal correction and the practical correction. The energy to be minimized can be written as

$$\begin{aligned} C = \int_0^{X_d}\int_0^{Y_d} \big(g_x(\bar{x}_d, \bar{y}_d) - \bar{x}_u\big)^2 \\ + \big(g_y(\bar{x}_d, \bar{y}_d) - \bar{y}_u\big)^2 \mathrm{d}x_d \mathrm{d}y_d \end{aligned} \tag{8}$$

The distortion center being known, the unknown parameters are the parameters in g_x and g_y. In practice, the simulation is performed on M samples $(x_{u_i}, y_{u_i}), i = 1, \cdots, M$ regularly distributed on an image. The corresponding distorted samples $(x_{d_i}, y_{d_i}), i = 1, \cdots, M$ are obtained by Eq (6). The discrete energy to be minimized is

$$D = \sum_{i=1}^{M} D_i^2 = \sum_{i=1}^{M} \left(g_x(\bar{x}_{d_i}, \bar{y}_{d_i}) - \bar{x}_{u_i}\right)^2 + \\ + \left(g_y(\bar{x}_{d_i}, \bar{y}_{d_i}) - \bar{y}_{u_i}\right)^2 \tag{9}$$

For radial model and polynomial model, this problem can be formularized as a linear system by computing the derivatives of D with respect to unknown parameters respectively and setting them to zero:

$$\mathbf{A}\mathbf{k} = \mathbf{b} \tag{10}$$

with $\mathbf{A}$ the coefficient matrix, $\mathbf{k}$ the unknown coefficient vector. The optimal solution minimizing the norm $\|\mathbf{A}\mathbf{k}-\mathbf{b}\|$ is $\mathbf{k} = \left(\mathbf{A}^T\mathbf{A}\right)^{-1}\mathbf{A}^T\mathbf{b}$. In practice, the coefficient matrix $\mathbf{A}$ is ill-conditioned and can make the solution unstable. Two normalization techniques can be applied to make the linear system more stable.

The first strategy is to normalize the matrix $\mathbf{A}$ so that its entries do not vary a lot. This normalization is performed by multiplying $\mathbf{A}$ by normalization matrices $\mathbf{T}_1$ and $\mathbf{T}_2$,

$$\hat{\mathbf{A}}\hat{\mathbf{k}} = \mathbf{T}_2\mathbf{A}\mathbf{T}_1\left(\mathbf{T}_1^{-1}\mathbf{k}\right) = \mathbf{T}_2\mathbf{b}, \tag{11}$$

chosen so that the entries of $\mathbf{T}_2\mathbf{A}\mathbf{T}_1$ get closer to each other. Then the solution is $\mathbf{k} = \mathbf{T}_1\left(\hat{\mathbf{A}}^T\hat{\mathbf{A}}\right)^{-1}\hat{\mathbf{A}}^T\mathbf{T}_2\mathbf{b}$.

The second strategy is to directly normalize $\bar{x}_{d_i}$ and $\bar{y}_{d_i}$ so that the average value of r_{d_i} is equal to 1. The normalization factor is $\alpha = \frac{\sum_{i=1}^{M}\sqrt{\bar{x}_{d_i}^2+\bar{x}_{d_i}^2}}{M}$. Eq (10) can be directly solved, followed by a denormalization of estimated parameters.

For example, for the radial model of order 4 with coefficients $k_0', k_1', k_2', k_3', k_4'$, the model in Eq. (7) has the following form:

$$\begin{aligned} g_x(\bar{x}_d, \bar{y}_d) &= \bar{x}_d(k_0' + k_1' r_d + k_2' r_d^2 + k_3' r_d^3 + k_4' r_d^4) \\ g_y(\bar{x}_d, \bar{y}_d) &= \bar{y}_d(k_0' + k_1' r_d + k_2' r_d^2 + k_3' r_d^3 + k_4 r_d^4) \end{aligned} \tag{12}$$

By some simple computations, the linear system in Eq. (10) can be explicitly written as:

$$\begin{aligned} \mathbf{A}\mathbf{k} &= \begin{bmatrix} \sum_i r_{d_i}^2 & \sum_i r_{d_i}^3 & \sum_i r_{d_i}^4 & \sum_i r_{d_i}^5 & \sum_i r_{d_i}^6 \\ \sum_i r_{d_i}^3 & & \cdots & & \sum_i r_{d_i}^7 \\ \vdots & & \ddots & & \vdots \\ \sum_i r_{d_i}^6 & & \cdots & & \sum_i r_{d_i}^{10} \end{bmatrix} \begin{pmatrix} k_0' \\ k_1' \\ k_2' \\ k_3' \\ k_4' \end{pmatrix} \\ = \mathbf{b} &= \begin{pmatrix} \sum_i r_{d_i}^2 \left(\bar{x}_{u_i}\bar{x}_{d_i} + \bar{y}_{u_i}\bar{y}_{d_i}\right) \\ \sum_i r_{d_i}^3 \left(\bar{x}_{u_i}\bar{x}_{d_i} + \bar{y}_{u_i}\bar{y}_{d_i}\right) \\ \sum_i r_{d_i}^4 \left(\bar{x}_{u_i}\bar{x}_{d_i} + \bar{y}_{u_i}\bar{y}_{d_i}\right) \\ \sum_i r_{d_i}^5 \left(\bar{x}_{u_i}\bar{x}_{d_i} + \bar{y}_{u_i}\bar{y}_{d_i}\right) \\ \sum_i r_{d_i}^6 \left(\bar{x}_{u_i}\bar{x}_{d_i} + \bar{y}_{u_i}\bar{y}_{d_i}\right) \end{pmatrix}. \end{aligned} \tag{13}$$

The entries of $\mathbf{A}$ differ by a big ratio $\frac{\sum_i r_{d_i}^{10}}{\sum_i r_{d_i}^2}$, which implies the numerical instability of the linear system. The normalization matrix $\mathbf{T}_1$ and $\mathbf{T}_2$ to lessen the instability in Eq. (11) can also be computed explicitly:

$$\mathbf{T}_1 = \begin{bmatrix} \frac{1}{\sum_i r_{d_i}^2} & 0 & 0 & 0 & 0 \\ 0 & \frac{1}{\sum_i r_{d_i}^3} & \cdots & & 0 \\ \vdots & & \ddots & & \vdots \\ 0 & \cdots & & & \frac{1}{\sum_i r_{d_i}^6} \end{bmatrix} \tag{14}$$

$$\mathbf{T}_2 = \begin{bmatrix} 1 & 0 & 0 & 0 & 0 \\ 0 & \frac{\sum_i r_{d_i}^2}{\sum_i r_{d_i}^3} & \cdots & & 0 \\ \vdots & & \ddots & & \vdots \\ 0 & \cdots & & & \frac{\sum_i r_{d_i}^2}{\sum_i r_{d_i}^6} \end{bmatrix}.$$

The same procedures can be used to test the universality of models. Only the polynomial model and the radial model (with fixed distortion center) can be solved by a linear method. For all the other models, a non-linear method must be used, even if (x_c, y_c) is known. The minimization is performed by first doing an incremental Levenberg-Marquardt (LM) algorithm which estimates the parameters in increasing order. The algorithm starts estimating the parameters of a low order model; the result is used to initialize the model 1 order higher, and the process continues until the aimed order. The Jacobian matrix $\mathbf{J}$, the partial derivative of each signed energy component D_i ($i = 1, \cdots, M$) with respect to each unknown parameter k'_j ($j = 1, \cdots, N$), is computed explicitly to make the incremental LM algorithm efficient:

$$\mathbf{J} = \begin{bmatrix} \frac{\partial D_1}{\partial k'_0} & \frac{\partial D_1}{\partial k'_1} & \cdots & \frac{\partial D_1}{\partial k'_{N-1}} & \frac{\partial D_1}{\partial k'_N} \\ \frac{\partial D_2}{\partial k'_0} & \frac{\partial D_2}{\partial k'_1} & \cdots & \frac{\partial D_2}{\partial k'_{N-1}} & \frac{\partial D_2}{\partial k'_N} \\ \vdots & & \ddots & & \vdots \\ \frac{\partial D_M}{\partial k'_0} & \frac{\partial D_M}{\partial k'_1} & \cdots & \frac{\partial D_M}{\partial k'_{N-1}} & \frac{\partial D_M}{\partial k'_N} \end{bmatrix}.$$

The self-consistency and universality are recapitulated in Table 2 and the parameters for generating distortion are in Table 1. $M = 5104$ points were regularly distributed in an image domain of size 1761×1174. They were first distorted by applying one kind of distortion (indicated in the entry row of Table 2) and then corrected by another model (indicated in the entry column of Table 2). The distortion center was fixed at the center $(880.5, 587)$ of the image and was assumed to be known. Table 2 shows the average error $\bar{D}$ and the maximal error D_∞:

$$\bar{D} = \sqrt{D(k'_0, k'_1, k'_2, \cdots)/M} \tag{15}$$

$$D_\infty = \max_i |D_i(k'_0, k'_1, k'_2, \cdots)| \tag{16}$$

after estimating the parameters $k'_0, k'_1, k'_2, \cdots$ which minimize the energy in Eq (9).

Rational function model Rational function model is an exception. In [10], rational function model is solved linearly by using some technique called "lifted process". This model is in fact designed to recover the 3D point $\mathbf{d}(i,j)$ on the *normalized image plane* represented in camera based coordinate system from the distorted point (i,j). $\mathbf{d}(i,j)$ is on the line passing through the undistorted point and the optic center:

$$\begin{aligned}\mathbf{d}(i,j) &= \mathbf{A}\mathcal{X}(i,j) \\ &= \begin{pmatrix}\mathbf{A}_{11}i^2 + \mathbf{A}_{12}ij + \cdots + \mathbf{A}_{15}j + \mathbf{A}_{16} \\ \mathbf{A}_{21}i^2 + \mathbf{A}_{22}ij + \cdots + \mathbf{A}_{25}j + \mathbf{A}_{26} \\ \mathbf{A}_{31}i^2 + \mathbf{A}_{32}ij + \cdots + \mathbf{A}_{35}j + \mathbf{A}_{36}\end{pmatrix}\end{aligned} \tag{17}$$

where $\mathcal{X}(i,j) = (i^2, ij, j^2, i, j, 1)^T$ the "lifted" coordinate of distorted image point $(i,j) = (x_d, y_d)$; $\mathbf{A}$ the extended camera calibration matrix:

$$\mathbf{A} = \begin{bmatrix}\mathbf{A}_{11} & \mathbf{A}_{12} & \mathbf{A}_{13} & \mathbf{A}_{14} & \mathbf{A}_{15} & \mathbf{A}_{16} \\ \mathbf{A}_{21} & \mathbf{A}_{22} & \mathbf{A}_{23} & \mathbf{A}_{24} & \mathbf{A}_{25} & \mathbf{A}_{26} \\ \mathbf{A}_{31} & \mathbf{A}_{32} & \mathbf{A}_{33} & \mathbf{A}_{34} & \mathbf{A}_{35} & \mathbf{A}_{36}\end{bmatrix}. \tag{18}$$

If there is no distortion, $\mathbf{A}$ is degenerated to be the inverse of camera calibration matrix $\mathbf{K}^{-1}$. $\lambda\mathbf{d}(i,j)$ $(\lambda \neq 0)$ is the 3D back-projected ray, passing through the camera optic center and the undistorted 2D image point. The inhomogeneous coordinate of $\mathbf{d}(i,j)$ is $(p,q)^T$:

$$\begin{aligned} p &= \frac{\mathbf{A}_{11}i^2 + \mathbf{A}_{12}ij + \cdots + \mathbf{A}_{15}j + \mathbf{A}_{16}}{A_{31}i^2 + \mathbf{A}_{32}ij + \cdots + \mathbf{A}_{35}j + \mathbf{A}_{36}} \\ q &= \frac{\mathbf{A}_{21}i^2 + \mathbf{A}_{22}ij + \cdots + \mathbf{A}_{25}j + \mathbf{A}_{26}}{A_{31}i^2 + \mathbf{A}_{32}ij + \cdots + \mathbf{A}_{35}j + \mathbf{A}_{36}}\end{aligned} \tag{19}$$

which is the coordinate of undistorted image point on *normalized image plane* (not on the physical CCD image plane). There is an unknown homography between the corrected point by rational function model and the undistorted point in image plane. In practice, the undistorted point in image plane is what we are looking for and is not available. To solve the matrix $\mathbf{A}$, a planar pattern containing known feature points $\mathbf{x}_i$ can be used. The extended calibration matrix $\mathbf{A}$ is a bridge linking $\mathbf{x}_i$ and the lift correspondence $\mathcal{X}_i$:

$$\begin{aligned} \mathbf{H}\mathbf{x}_i &= \lambda_i\mathbf{A}\mathcal{X}_i \\ \iff \mathbf{x}_i &= \lambda_i\mathbf{H}^{-1}\mathbf{A}\mathcal{X}_i = \lambda_i\mathbf{A}'\mathcal{X}_i \\ \iff [\mathbf{x}_i]_\times\mathbf{A}'\mathcal{X}_i &= \mathbf{0}\end{aligned} \tag{20}$$

Recall that $\mathbf{A}\mathcal{X}_i$ is homogeneous coordinate of the projection of 3D point on the normalized image plane. So here the unknown homography $\mathbf{H}$ sends the points from the pattern to the normalized image plane. $\mathbf{A}' = \mathbf{H}^{-1}\mathbf{A}$ will recover the point on the original pattern. One pair of correspondence gives two equations for $\mathbf{A}'$, so 9 pairs of correspondences are sufficient to estimate $\mathbf{A}'$. Note that if $\mathbf{A}$ rectifies camera to pinhole, does $\mathbf{A}'$ also even with the hidden $\mathbf{H}$. This linear algorithm can be directly applied in our synthetic test, where the known undistorted points replace the points on the pattern.

But like many other linear algortihms in multi-view geometry, this "lifted technique" minimizes the algebraic error, which is not directly related to the geometric error. Sometimes a small algebraic error can give a big geometric error. So in the simulation, the parameters of rational function model are still estimated by the incremental LM algorithm by using the result of linear "lifted technique" as an initialization.

model	parameters
radial 2° $1084 \rightarrow 1050$	$k_0 = 1.0$, $k_1 = 0.25\text{e}{-4}$, $k_2 = -0.5\text{e}{-7}$
radial 4° $991.6 \rightarrow 1050$	$k_0 = 1.0$, $k_1 = 0.25\text{e}{-4}$, $k_2 = -0.5\text{e}{-7}$, $k_3 = 1.0\text{e}{-10}$, $k_4 = -1.5\text{e}{-14}$
division 2° $1083 \rightarrow 1050$	$d_0 = 1.0$, $d_1 = -0.25\text{e}{-4}$, $d_2 = 0.5\text{e}{-7}$
division 4° $988.7 \rightarrow 1050$	$d_0 = 1.0$, $d_1 = -0.25\text{e}{-4}$, $d_2 = 0.5\text{e}{-7}$, $d_3 = -1.0\text{e}{-10}$, $d_4 = 1.5\text{e}{-14}$
FOV 3° $501.4 \rightarrow 1050$	$k_0 = 1.0$, $\omega = 1.0 \times 10^{-3}$, $k_2 = -2.0 \times 10^{-7}$, $k_3 = 4.0 \times 10^{-10}$
polynomial 3° $1050 \rightarrow 1064$	$a_1 = b_1 = -1.0\text{e}{-8}, \cdots, a_5 = b_5 = 2.0\text{e}{-5}, \cdots,$ $a_8 = 0.9$, $a_9 = 0.1$, $a_{10} = 0.0$, $b_8 = 0.1$, $b_9 = 0.9$, $b_{10} = 0.0$
polynomial 4° $1050 \rightarrow 1075$	$a_1 = b_1 = 5.0\text{e}{-12}$, $a_6 = b_6 = -1.0\text{e}{-8}$, $a_{10} = b_{10} = 2.0\text{e}{-5}, \cdots,$ $a_{13} = 0.9$, $a_{14} = 0.1$, $a_{15} = 0.0$, $b_{13} = 0.1$, $b_{14} = 0.9$, $b_{15} = 0.0$
rational 2° $1031 \rightarrow 1104$	$a_1 = 1.0 \times 10^{-5}$, $a_2 = 2.0 \times 10^{-5}$, $a_3 = 3.0 \times 10^{-5}$, $a_4 = 0.9$, $a_5 = 0.1$, $a_6 = 0.0$ $b_1 = 3.0 \times 10^{-5}$, $b_2 = 2.0 \times 10^{-5}$, $b_3 = 1.0 \times 10^{-5}$, $b_4 = 0.1$, $b_5 = 0.9$, $b_6 = 0.0$ $c_1 = 1.0 \times 10^{-8}$, $c_2 = 1.0 \times 10^{-8}$, $c_3 = 1.0 \times 10^{-8}$, $c_4 = 0.0001$, $c_5 = 0.0001$, $c_6 = 1.0$

Table 1: Models used to generate distortion, with their realistic parameters. The values on the left and on the right of $\rightarrow$ are the undistorted radius and the distorted radius respectively. For the polynomial model, the coefficients are the same for x and y component, except for the order 1 coefficients. Note that the distortion can be barrel, pincushion or mustache.

3.2 Experiments with unknown distortion center

In practice, the distortion center (x_c, y_c) is unknown. It should also be considered as a parameter in the minimization formulation. The minimization problem becomes non-linear for most models if (x_c, y_c) is unknown. This is true for the radial model, the division model, the FOV model and the rational model. In contrast the polynomial and the rational function models are invariant to a translation of the distortion center. The point (x_c, y_c) can be fixed arbitrarily, and in the polynomial case the minimization problem is linear while the rational model is still non-linear. This is a decisive advantage with respect to the other models. The self-consistency and universality results are recapitulated in Table 3 with the parameters for generating distortion in Table 1. For the distortion generation, the distortion center was fixed at the center $(880.5, 587)$ of the image, while for the correction,

	R 2°	R 4°	D 2°	D 4°	F 3°	P 3°	P 4°	Ra 2°
R 2°	9e−2/8e−1	1e−1/4e−1	6e−2/5e−1	2e−1/5e−1	3e−2/1e−1	6e+1/2e+2	6e+1/2e+2	7e+1/2
R 4°	2e−3/3e−2	2e−3/2e−2	8e−4/9e−3	2e−3/8e−3	8e−4/6e−3	6e+1/2e+2	6e+1/2e+2	7e+1/2
D 2°	6e−2/6e−1	2e−1/6e−1	3e−2/3e−1	2e−1/1e+0	4e−2/2e−1	6e+1/2e+2	6e+1/2e+2	7e+1/2
D 4°	1e−3/2e−2	1e−3/9e−3	4e−4/4e−3	1e−3/7e−3	7e−4/6e−3	6e+1/2e+2	6e+1/2e+2	7e+1/2
F 3°	8e−2/3e−1	7e−2/8e−1	9e−2/4e−1	6e−2/7e−1	2e−2/2e−1	6e+1/2e+2	6e+1/2e+2	7e+1/2
P 3°	6e−1/3e+0	5e−1/2e+0	5e−1/3e+0	6e−1/3e+0	2e−1/8e−1	2e−1/2e+0	7e−1/6e+0	5e−1/3
P 4°	6e−1/3e+0	5e−1/2e+0	5e−1/3e+0	6e−1/3e+0	2e−1/8e−1	5e−2/6e−1	1e−1/2e+0	7e−2/6
P 8°	6e−2/4e−1	2e−2/1e−1	6e−2/4e−1	2e−2/1e−1	7e−3/6e−2	7e−5/1e−3	7e−4/1e−2	4e−5/6
P 15°	1e−2/6e−2	8e−3/5e−2	1e−2/6e−2	8e−3/5e−2	3e−4/1e−3	1e−7/7e−7	2e−7/3e−6	4e−7/4
Ra2°	5e+0/2e+1	7e+0/3e+1	5e+0/2e+1	7e+0/3e+1	4e+1/1e+3	5e−1/3e+0	4e−1/1e+0	1e−1/8
Ra6°	5e−2/2e−1	3e−2/2e−1	1e−1/7e−1	9e−2/7e−1	1e−1/6e−1	2e−6/3e−5	1e−4/2e−3	8e−8/9
Ra10°	4e−2/2e−1	2e−2/1e−1	1e−1/8e−1	9e−2/7e−1	3e−2/3e−1	8e−8/1e−6	2e−7/3e−6	4e−9/5

Table 2: Self-consistency and universality with known distortion center. The average error ($\bar{D}$)/maximal error (D_∞) (in pixels) is shown. The left column entries show the model and the order used for correction. The top entry row gives the model and the order used to generate the distortion. The five compared model classes are R-Radial, D-Division, F-FOV, P-Polynomial, and Ra-Rational. The parameters in Table 1 were used to generate the distortion. The green color is used to highlight the average error $\bar{D} \leqslant 10^{-2}$, the blue color for $10^{-2} < \bar{D} \leqslant 10^{-1}$ and the red color for $\bar{D} > 10^{-1}$.

the initial distortion center was realistically taken $(50, 50)$ pixels away from the true position. For the radial model and the division model, the Levenberg-Marquardt algorithm could still find the true distortion center, and the minimized error was the same as when the distortion center was known. Nevertheless, for the FOV model, a bad initialization of the distortion center degraded the correction performance. For the polynomial model, the solution can be found linearly by fixing an arbitrary distortion center. For rational function model, even though it is invariant to a translation of the distortion center, incremental LM algorithm cannot ensure the correct minimization.

3.3 Comparison

The tables show that the models are self-consistent for an average precision of the order of 10^{-2} pixel if the order of correction is high enough when the distortion center is known. The radial model and the division model are consistent with each other, whether the distortion center is known or not. The FOV model is a little less consistent with the radial model and the division model when the distortion center is known. With an unknown distortion center, the FOV correction performance decays. The polynomial model instead seems to be able to correct any type of distortion, but a higher order is often necessary to correct the radial, division or FOV distortions. This higher order is not a

	R 2°	R 4°	D 2°	D 4°	F 3°	P 3°	P 4°	Ra 2°
R 2°	9e−2/8e−1	1e−1/4e−1	6e−2/5e−1	2e−1/5e−1	3e−2/1e−1	6e+1/2e+2	6e+1/2e+2	7e+1/2
R 4°	2e−3/3e−2	2e−3/2e−2	8e−4/9e−3	2e−3/8e−3	8e−4/6e−3	6e+1/2e+2	6e+1/2e+2	7e+1/2
D 2°	6e−2/6e−1	2e−1/6e−1	3e−2/3e−1	2e−1/1e+0	4e−2/2e−1	6e+1/2e+2	6e+1/2e+2	7e+1/2
D 4°	1e−3/2e−2	1e−3/9e−3	4e−4/4e−3	1e−3/7e−3	2e+1/4e+1	6e+1/2e+2	6e+1/2e+2	7e+1/2
F 3°	7e−1/2e+0	3e+0/2e+1	2e+0/9e+0	3e+0/2e+1	4e+1/6e+1	6e+1/2e+2	6e+1/2e+2	7e+1/2
P 3°	6e−1/3e+0	5e−1/2e+0	5e−1/3e+0	6e−1/3e+0	2e−1/8e−1	2e−1/2e+0	7e−1/6e+0	5e−1/3
P 4°	6e−1/3e+0	5e−1/2e+0	5e−1/3e+0	6e−1/3e+0	2e−1/8e−1	5e−2/6e−1	1e−1/2e+0	7e−2/6
P 8°	6e−2/4e−1	2e−2/1e−1	6e−2/4e−1	2e−2/1e−1	7e−3/6e−2	7e−5/1e−3	7e−4/1e−2	4e−5/6
P 15°	1e−2/6e−2	8e−3/5e−2	1e−2/6e−2	8e−3/5e−2	3e−4/1e−3	1e−7/7e−7	2e−7/3e−6	4e−7/4
Ra2°	7e+1/9e+1	7e+1/1e+2	7e+1/9e+1	7e+1/1e+2	7e+1/8e+1	7e+1/7e+1	7e+1/7e+1	7e+1/7
Ra6°	7e+1/7e+1	7e+1/7e+1	7e+1/7e+1	7e+1/7e+1	7e+1/7e+1	7e+1/7e+1	7e+1/7e+1	7e+1/7
Ra10°	7e+1/7e+1	7e+1/7e+1	7e+1/7e+1	7e+1/7e+1	7e+1/7e+1	7e+1/7e+1	7e+1/7e+1	7e+1/7

Table 3: Self-consistency and universality with unknown distortion center. The initial distortion center was set $(50, 50)$ pixels away from its true position. The average error $(\bar{D})$/maximal error (D_∞) (in pixels) is shown. The left column entries give the model and the order used for correction. The top row entries give the model and the order used to generate the distortion. The five compared model classes are R-Radial, D-Division, F-FOV, P-Polynomial, and Ra-Rational. The parameters in Table 1 were used to generate the distortion. The green color is used to highlight the average error $\bar{D} \leqslant 10^{-2}$, the blue color for $10^{-2} < \bar{D} \leqslant 10^{-1}$ and the red color for $\bar{D} > 10^{-1}$.

problem, because of the computational efficiency of the linear method. The rational function model should have the same performance as the polynomial model. But due to the complexity in non-linear minimization, sometimes it is often stuck by the local minima. In conclusion, the polynomial model is the only one to be jointly self-consistent, universal and linear among the compared models.

3.4 Realistic distortion

A real distortion can be far more complex than what the above simple models can generate. A more realistic distortion contains a radial symmetric term, a term for decentering distortion and a term for thin prism distortion [28],

$$\begin{aligned}\bar{x}_d &= \bar{x}_u \left(k_0 + k_1 r_u + k_2 r_u^2 + \cdots\right) \\ &+ \left[p_1 \left(r_u^2 + 2\bar{x}_u^2\right) + 2p_2 \bar{x}_u \bar{y}_u\right] \left(1 + p_3 r_u^2\right) + s_1 r_u^2 \\ \bar{y}_d &= \bar{y}_u \left(k_0 + k_1 r_u + k_2 r_u^2 + \cdots\right) \\ &+ \left[p_2 \left(r_u^2 + 2\bar{y}_u^2\right) + 2p_1 \bar{x}_u \bar{y}_u\right] \left(1 + p_3 r_u^2\right) + s_2 r_u^2\end{aligned}$$

with p_1, p_2, p_3 parameters for decentering distortion and s_1, s_2 parameters for thin prism distortion. They are both tangential distortions. In Table 4, the self-consistency and universality of the models were again tested with known distortion center after adding a tangential distortion with $p_1 = 4.0\text{e}{-6}, p_2 = -2.0\text{e}{-6}, p_3 = 0, s_1 = 3.0\text{e}{-6}, s_2 = 1.0\text{e}{-6}$. By adding this non-radial component in the distortion, the radial model, the division model and the FOV model do not reach anymore the 10^{-2} pixel precision. The rational function model again has the minimization problem. The polynomial model is the only model getting a higher precision when increasing the model order.

4 Real distortion fitting experiments

After its validation on synthetic examples, we present here real tests to verify that the proposed high order polynomial model works for real distortion correction. This test was inspired from the non-parametric lens distortion estimation method in [11] but could be performed on any distortion model obtained by blind correction. This method requires a highly textured planar pattern, which is obtained by printing a textured image and pasting it on a very flat object (a mirror was used in the experiments). Two photos of the pattern were taken by a Canon EOS 30D SLR camera with EFS $18-55$mm lens. The minimal focal length (18mm) was chosen (with fixed focus) to produce a fairly large distortion. The distortion was estimated (up to a homography) as the diffeomorphism mapping the original digital pattern to a photograph of it. The algorithm is summarized in the following without going into details.

1. Take two slightly different photographs of a textured planar pattern with a camera whose settings are frozen;

	R 2°	R 4°	D 2°	D 4°	F 3°	P 3°	P 4°	Ra 2°
R 2°	7e+0/3e+1	5e+0/2e+1	7e+0/3e+1	5e+0/2e+1	7e−1/2e+0	6e+1/2e+2	6e+1/2e+2	7e+1/2
R 4°	7e+0/3e+1	5e+0/2e+1	7e+0/3e+1	5e+0/2e+1	7e−1/2e+0	6e+1/2e+2	6e+1/2e+2	7e+1/2
D 2°	7e+0/3e+1	5e+0/2e+1	7e+0/3e+1	5e+0/1e+1	7e−1/2e+0	6e+1/2e+2	6e+1/2e+2	7e+1/2
D 4°	7e+0/3e+1	5e+0/2e+1	7e+0/3e+1	5e+0/2e+1	7e−1/2e+0	6e+1/2e+2	6e+1/2e+2	7e+1/2
F 3°	7e+0/3e+1	5e+0/2e+1	7e+0/3e+1	5e+0/2e+1	7e−1/2e+0	6e+1/2e+2	6e+1/2e+2	7e+1/2
P 3°	6e−1/4e+0	5e−1/4e+0	5e−1/4e+0	6e−1/4e+0	2e−1/9e−1	3e−1/3e+0	8e−1/7e+0	3e−1/2
P 4°	6e−1/3e+0	5e−1/2e+0	5e−1/3e+0	6e−1/3e+0	2e−1/8e−1	6e−2/7e−1	2e−1/2e+0	5e−2/4
P 8°	6e−2/4e−1	2e−2/1e−1	6e−2/4e−1	2e−2/1e−1	7e−3/6e−2	1e−4/2e−3	1e−3/2e−2	1e−5/2
P 15°	1e−2/6e−2	8e−3/5e−2	1e−2/6e−2	8e−3/5e−2	3e−4/2e−3	3e−7/2e−6	3e−7/6e−6	3e−7/4
Ra2°	5e+0/2e+1	7e+0/3e+1	5e+0/2e+1	7e+0/3e+1	3e+0/1e+1	6e−1/3e+0	4e−1/1e+0	1e−1/8
Ra6°	1e−1/9e−1	1e−1/8e−1	1e−1/9e−1	9e−2/8e−1	3e−2/3e−1	2e−6/3e−5	2e−4/2e−3	3e−7/5
Ra10°	1e−1/9e−1	1e−1/8e−1	1e−1/8e−1	9e−2/7e−1	3e−2/2e−1	8e−8/1e−6	3e−7/5e−6	3e−9/6

Table 4: Self-consistency and universality with known distortion center. Compared with Tables 2 and 3, besides the distortion generated by the parameters in Table 1, an additional tangential distortion is added. Each entry shows the average error ($\bar{D}$)/maximal error (D_∞) (in pixels). The green color is used to highlight the average error $\bar{D} \leqslant 10^{-2}$, the blue color for $10^{-2} < \bar{D} \leqslant 10^{-1}$ and the red color for $\bar{D} > 10^{-1}$. The only blue-green to green lines are obtained for the polynomial model with degree 8 to 15.

2. apply SIFT method [19] between the original digital pattern and both photographs to find matchings;
3. eliminate outliers by a loop validation step;
4. triangulate and interpolate the remaining matchings to get a dense reverse distortion field;
5. refine the precision of the SIFT matchings by moving each point in one image by applying the local homography estimated from its neighboring matchings;
6. by applying the reverse distortion field to all images produced by the real camera, the camera is converted into a virtual pinhole camera.

The matchings delivered by step 5 (about 8000 matchings in our experiments) in the above algorithm are "outliers"-free and precise thanks to the loop validation and local homography. So we can directly try all models to fit these "outliers"-free matchings. The residual fitting error shows to what extent the models are faithful to a real camera lens distortion. In addition, there is an arbitrary homography between the digital pattern and its photograph. So the compatibility of the models with a homography is also implicitly tested. We used 50% matchings to estimate the parameters for different models and the other 50% to evaluate the fitting error. The results are recapitulated in Table 5, compared to the non-parametric method [11]. They show that all of the radial symmetric models fail (including the radial, division and

FOV models) because the distortion field is not radial symmetric due to the implicit unknown homography. In this experiment, the rational model gives a performance similar to the polynomial model *by chance* (in contrast in synthetic test, the incremental LM algorithm does not find a global minima). The fitting error of the polynomial model becomes stable when its order attains 7, which means that it does not suffer from numerical instability or noise fitting. *The precision attained with the polynomial model is about 500 times higher than with classic models!* The non-parametric method gives a slightly larger fitting error than the polynomial model because the triangulation (step 4 in the above summarized algorithm) at the border of image can be imprecise (see the difference at the border for non-parametric method and the polynomial model in Fig. 4 and 3).

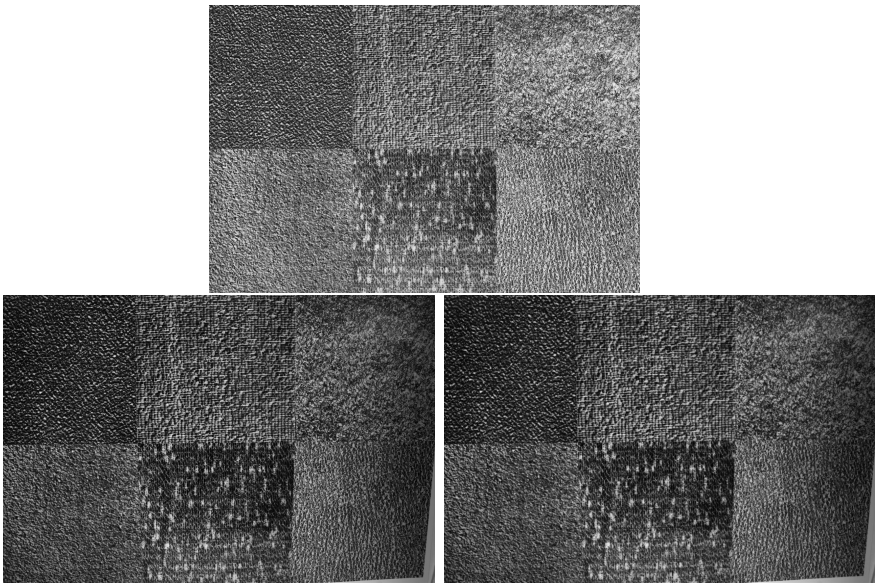

Figure 2: The textured pattern and two photos. Top row: the digital textured pattern. Bottom row: two similar photos of the pattern.

5 Plumb-line validation

It should be noted that the non-parametric method does not give a ground truth. It is just a non-parametric estimation of the lens distortion, and it is subject to errors. These errors are evident in that the non-parametric model has a mean fitting error of 0.18 pixels. Thus, we need a more objective evaluation to check the quality of the correction polynomial model. To this purpose, a physical frame with tightly stretched cylindrical strings was built. The physical tension of the strings guarantees a very high straightness. Once the parameters of

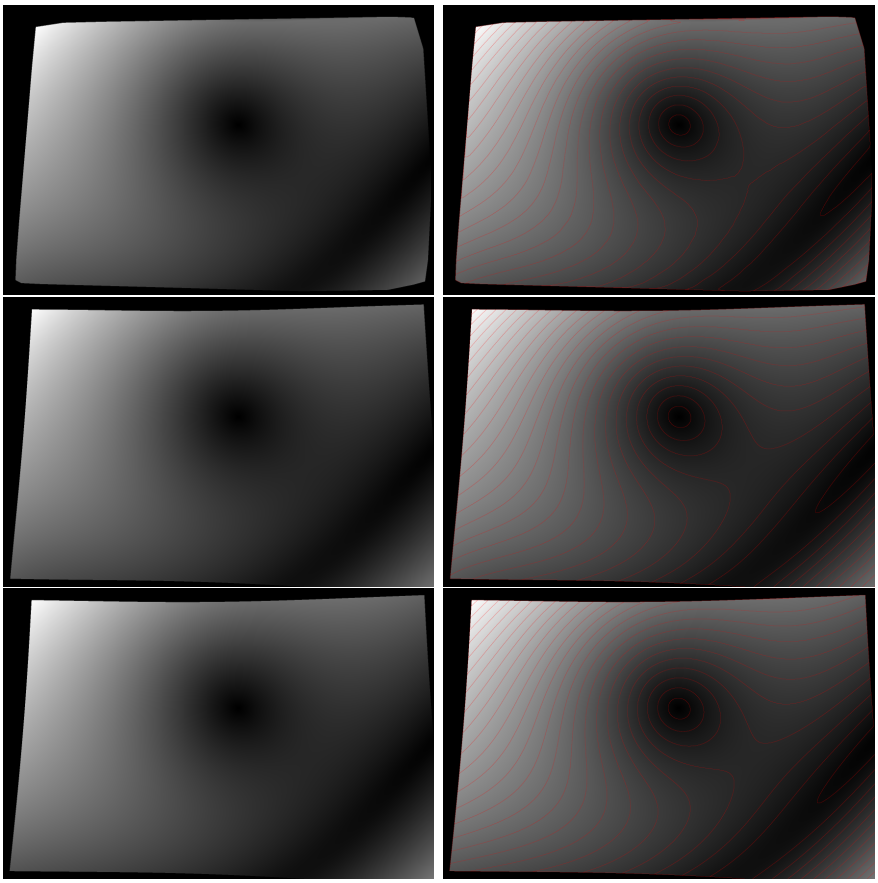

Figure 3: The distortion field estimated by different methods. Top row: the distortion field obtained by a non-parametric method [11] and its level lines (in red) with quantization step 20. Middle row: the distortion field constructed by the estimated parameters of polynomial model of order-12 and the level lines (in red) with quantization step of 20. Bottom row: the distortion field constructed by the estimated parameters of rational function model of order-12 and the level lines (in red) with quantization step of 20.

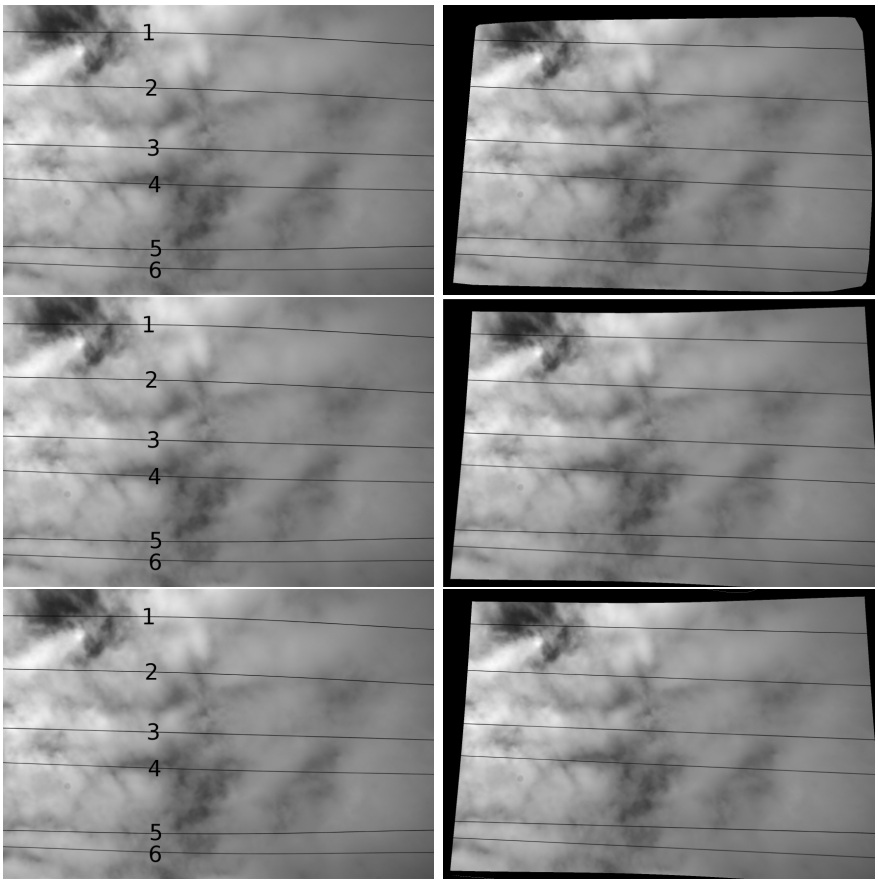

Figure 4: Top row: distorted image of tightly stretched lines and the corrected image by the non-parametric method. Middle row: distorted images of tightly stretched lines and the corrected image by the estimated polynomial model. Bottom row: distorted images of tightly stretched lines and the corrected image by the estimated rational function model.

order	Parametric model type					Non-parametric model [11]
	Radial	Division	FOV	Polynomial	Rational	
3	24.66/89.84	26.98/103.30	26.72/101.74	1.48/10.65	0.19/1.86	0.18/6.21
4	24.55/89.08	26.95/103.22	25.47/94.53	1.26/8.93	0.05/0.49	
5	24.30/85.74	26.94/104.32	25.48/95.17	0.21/2.09	0.05/0.33	
6	24.28/85.58	25.43/94.53	25.47/94.87	0.08/0.83	0.05/0.27	
7	24.29/85.45	24.37/86.58	25.17/93.22	0.04/0.35	0.04/0.24	
8	24.27/85.93	24.27/85.87	25.18/93.66	0.04/0.27	0.04/0.87	
9	24.28/86.07	24.28/86.14	25.15/93.63	0.04/0.25	0.04/0.39	
10	24.27/86.24	24.28/86.21	24.28/86.03	0.04/0.22	0.04/0.39	
11	24.26/86.64	24.26/86.62	24.27/86.52	0.04/0.22	0.04/0.39	
12	24.27/86.48	24.27/86.53	24.26/86.57	0.04/0.26	0.04/0.39	

Table 5: The fitting error (in pixels) of the compared models to the matchings between a digital textured image and its photograph. The matchings obtained at step 5 in the summarized algorithm are "outliers"-free and precise. Column 1 is the order of the model. 50% matchings are used to estimate the parameters and the shown average/maximal fitting error is computed on the other 50% matchings by applying the estimated parameters. The fitting error of non-parametric method in the last column is computed in the same manner: 50% matchings are fist used to estimate the deformation field, and the other 50% matchings are used to compute the fitting error the estimated deformation field.

the models are estimated, a distortion field can be constructed and applied for the distortion correction of images of strings taken by the same camera with the same fixed lens configuration (see Fig. 4). The average/max distance from the edge points (computed by the method of [7]) of the corrected lines to the corresponding regression line was computed. Table 6 recapitulates average/max distance for all lines in the image. The polynomial model still gives a stable performance when the order attains 6, *which means that a polynomial model of order* 6 *was already capable of capturing the whole distortion.* The residual fitting error comes from the noise of matching points. The polynomial model has far too few parameters to fit this noise, which guarantees the correction quality and stability. The rational model gives a comparable performance at the price of much higher computational cost (more than 200 times slower). All of the other parametric models do not give a satisfying result for the reason explained above (their average/max error is in fact larger than shown because the used line segment detector [22] sometimes detects only one part of the non-corrected lines). The non-parametric method gives a performance very close to the polynomial model, which confirms again the effectiveness of polynomial model (see Fig. 4 for the visual inspection).

order	Parametric model type					Non-parametric model [11]
	Radial	Division	FOV	Polynomial	Rational	
3	6.86/36.96	3.77/21.13	4.06/20.70	0.74/4.36	0.11/0.77	0.09/0.44
4	6.91/33.70	3.85/21.75	5.80/33.49	0.58/2.47	0.09/0.51	
5	7.61/32.86	3.78/19.09	5.83/30.72	0.15/0.51	0.09/0.50	
6	7.65/33.58	5.92/29.95	5.89/29.90	0.09/0.45	0.09/0.49	
7	5.53/24.94	6.39/31.21	6.30/33.42	0.09/0.51	0.09/0.49	
8	7.60/32.91	7.59/33.11	5.68/25.26	0.09/0.52	0.09/0.49	
9	6.69/26.71	6.78/26.95	5.83/26.64	0.09/0.52	0.09/0.51	
10	5.42/21.54	6.16/26.11	7.55/33.62	0.09/0.55	0.09/0.52	
11	2.33/8.85	2.38/8.65	3.11/11.30	0.09/0.52	0.09/0.52	
12	1.72/5.15	1.53/4.36	1.95/6.67	0.09/0.51	0.09/0.52	

Table 6: The average/max distance (in pixels) from edge points of corrected lines to the corresponding regression line. The parameters of the models are estimated by 50% matchings coming from step 5 in the summarized algorithm. The distorted image in Fig. 4 is then corrected by using all models. The corrected lines are extracted by using the algorithm in [22], which is supposed to extract straight lines in images. Note that for the radial model, division model, FOV model, the correction is not satisfying. Sometimes only one part of or even no line can be extracted. So the error is bigger than shown. But all lines are reliably extracted from the image corrected by the polynomial model, rational model or the non-parametric method.

6 Conclusion

We introduced the self-consistency and universality criteria for camera lens distortion models. Using these tools, five classic distortion models were evaluated and compared. The polynomial and rational function model were shown to be both self-consistent and universal, to the cost of a high degree. This high degree raises no computational issue for the polynomial model. Indeed, we have seen that after a correct conditioning it can always be solved linearly. In contrast to the rational model needs to be solved by an incremental Levenberg-Marquardt algorithm initialized by a linear method (even though, it is not ensured that the complexe non-linear minimization always find a global minima). Furthermore, the polynomial model is translation invariant, which makes it insensitive to a translation of the distortion center. This model is not adapted to global camera calibration methods where the internal and external parameters and the distortion model are estimated simultaneously. The distortion correction must be dealt with as an independent and previous step to camera calibration. It might be objected that the high number of parameters in the polynomial interpolation (156 for an 11-order polynomial) could cause over-fitting bias in the results. Yet, the number of control points (about 4000) is far higher, about 30 times the number of polynomial coefficients. Our experiments show that the residual errors stabilize for orders between 6 to 12, confirming that no over-fitting occurred. Our experiments also show that high order polynomials are really needed if we wish to obtain high precisions. And they indeed deliver accuracies hundred to thousand times higher than those obtained with classic models.

References

[1] Luis Alvarez and J. Rafael Sendra. An algebraic approach to lens distortion by line rectification. *Journal of Mathematical Imaging and Vision*, 35:36–50, 2009.

[2] Duane C. Brown. Close-range camera calibration. *Photogrammetric Engineering*, 37:855–866, Brown.

[3] M. Byrod, Z. Kukelova, K. Josephson, T. Pajdla, and K. Astrom. Fast and robust numerical solutions to minimal problems for cameras with radial distortion. *Computer Vision and Image Understanding*, 114(2):1–8, 2008.

[4] D. Claus and A. W. Fitzgibbon. A plumbline constraint for the rational function lens distortion model. *BMVC*, pages 99–108, 2005.

[5] D. Claus and A.W. Fitzgibbon. A rational function lens distortion model for general cameras. *CVPR*, 1:213–219, 2005.

[6] Margaret M. Fleck Daniel Stevenson. Nonparametric correction of distortion. Technical report, omp. Sci., U. of Iowa, 1995.

[7] F. Devernay. A non-maxima suppression method for edge detection with sub-pixel accuracy. Technical Report 2724, INRIA rapport de recherche, 1995.

[8] F. Devernay and O. Faugeras. Straight lines have to be straight. *Mach. Vision Appli.*, 13:14–24, 2001.

[9] Hany Farid and Alin C. Popescu. Blind removal of lens distortion. *Journal of the Optical Society of America*, 2001.

[10] A. Fitzgibbon. Simultaneous linear estimation of multiple view geometry and lens distortion. *ICPR*, 1:125–132, 2001.

[11] R. Grompone von Gioi, P. Monasse, J.-M. Morel, and Z. Tang. Towards high-precision lens distortion correction. *ICIP*, pages 4237–4240, 2010.

[12] R. I. Hartley and T. Saxena. The cubic rational polynomial camera model. *Proc. DARPA Image Understanding Workshop*, pages 649–653, 1997.

[13] R.I Hartley and A. Zisserman. *Multiple View Geometry in Computer Vision*. Cambridge Univ. Press, 2000.

[14] E. Kilpelä. Compensation of systematic errors of image and model coordinates. *Photogrammetria*, 37(1):15–44, 1980.

[15] Z. Kukelova and T. Pajdla. A minimal solution to the autocalibration of radial distortion. *CVPR*, page 17, 2007.

[16] K. L. Moore L. Ma, Y. Chen. Rational radial distortion models of camera lenses with analytical solution for distortion correction. *International Journal Information Acquisition*, 1(2):135–147, 2004.

[17] Dhome M. Lavest J., Viala M. Do we really need accurate calibration pattern to achieve a reliable camera calibration. *ECCV*, 1:158–174, 1998.

[18] Hongdong Li and Richard Hartley. A non-iterative method for correcting lens distortion from nine point correspondences. *OmniVis*, 2005.

[19] David G Lowe. Distinctive image features from scale-invariant keypoints. *IJCV*, 60(2):91110, 2OO4.

[20] T. Pajdla, Z. Kukelova, and M. Bujnak. Automatic generator of minimal problem solvers. *ECCV*, pages 302–315, 2008.

[21] B. Prescott and G. F. Mclean. Line-based correction of radial lens distortion. *Graphical Models and Image Processing*, 59:39–47, 1997.

[22] J.-M. Morel G. Randall R. Grompone von Gioi, J. Jakubowicz. Lsd: A fast line segment detector with a false detection control. *IEEE Trans. on PAMI*, 99, 2008.

[23] Gideon P. Stein. Lens distortion calibration using point correspondences. *CVPR*, 602–608, 1997.

[24] J. G. Fryer T. A. Clarke. The development of camera calibration methods and models. *The Photogrammetric Record*, 16:51–66, 1998.

[25] M. Thirthala and S. Pollefeys. Multi-view geometry of 1d radial cameras and its application to omnidirectional camera calibration. *ICCV*, pages 1539–1546, 2005.

[26] Václav Hlaváč Tomáš Pajdla, Tomáš Werner. Correcting radial lens distortion without knowledge of 3-d structure. *Research Report, Czech Technical University*, 1997.

[27] Roger Y. Tsai. A versatile camera calibration technique for high-accuracy 3d machine vision metrology using off-the-shelf tv cameras and lenses. *IEEE Journal of Robotics and Automation*, Vol. RA-3, 1987.

[28] J. Weng, P. Cohen, and M. Herniou. Camera calibration with distortion models and accuracy evaluation. *TPAMI*, 14(10):965–980, 1992.

[29] A. Jakas Y. Liu, A. Al-Obaidi and L. Li. Accurate camera calibration and correction using rigidity and radial alignment constraints. *3DPVT*, pages 145–152, 2008.

[30] Z. Zhang. On the epipolar geometry between two images with lens distortion. *Proceedings of the 1996 International Conference on Pattern Recognition*, 7270:407, 1996.

[31] Z. Zhang. A flexible new technique for camera calibration. *ICCV*, pages 663–673, September 1999.